Chemical tuning of electrical transport in Ti_{1-x}Pt_{x}Se_{2-y}

Justin S. Chen, Jiakui K. Wang, Scott V. Carr, Sven C. Vogel, Olivier Gourdon, Pengcheng Dai, and E. Morosan

Phys. Rev. B **91**, 045125 — Published 20 January 2015

DOI: 10.1103/PhysRevB.91.045125

Remarkable chemical tuning of the electrical transport in $Ti_{1-x}Pt_xSe_{2-y}$

Justin S. Chen,[1] Jiakui K. Wang,[1] Scott V. Carr,[1] Sven C. Vogel,[2] Olivier Gourdon,[2] Pengcheng Dai,[1] and E. Morosan[1]

[1] *Department of Physics and Astronomy, Rice University, Houston, TX 77005, USA*
[2] *Los Alamos National Laboratory, Los Alamos Neutron Science Center, Los Alamos, New Mexico 87545, USA*

(Dated: December 16, 2014)

The structural and transport properties of polycrystalline $Ti_{1-x}Pt_xSe_{2-y}$ ($x \leq 0.13$, $y \leq 0.2$) are studied, revealing highly tunable electrical properties, spanning nearly 10 orders in magnitude in scaled resistivity. Using x-ray and neutron diffraction, Pt is found to dope on the Ti site. In the absence of Pt doping (for $x = 0$), Se deficiency ($y > 0$) increases the metallic character of $TiSe_2$, while a remarkable increase of the low temperature resistivity is favored by no Se deficiency ($y = 0$) and increasing amounts of doped Pt ($x > 0$). The chemical tuning of the resistivity in $Ti_{1-x}Pt_xSe_{2-y}$ with Se deficiency *and* Pt doping results in a metal-to-insulator transition. The simultaneous Pt doping and Se deficiency ($x,y > 0$) confirms the competition between the two opposing trends in electrical transport, with the main outcome being the suppression of the charge density wave (CDW) transition below 2 K for $y = 2x = 0.18$. Band structure calculations on a subset of $Ti_{1-x}Pt_xSe_{2-y}$ compositions are in line with the experimental observations.

PACS numbers: 71.30.+h,71.20.Nr,71.45.Lr

I. INTRODUCTION

Layered crystal structures with van der Waals gaps lend themselves to great tuning versatility. Particularly, the layered transition metal dichalcogenides (LTMD) are a family of two-dimensional compounds, with electrical transport properties ranging from metals to insulators, mostly with a charge density wave (CDW) ground state.[1] Chemical modifications of these systems include intercalation (in the van der Waals gaps) or substitution with magnetic or non-magnetic elements, greatly enhancing the range of physical properties observed in the LTMDs, to include unconventional superconductivity,[1–7] magnetism[7–10] or metal-insulator transitions.[3,11]

The layered crystal structure of the hexagonal LTMDs has prompted studies analogous to those in hexagonal graphene, particularly aiming the fabrication of electronic devices. MoS_2 in particular has attracted recent interest, as its properties can also be tuned through a variety of methods such as strain[12] or the application of electric fields.[13] The CDW state has been exploited in several LTMDs, mainly $TiTe_2$[14] and TaS_2,[15] to produce devices with non-linear I-V characteristics. There also was recent interest in $TiSe_2$, with new fabrication techniques using mechanical exfoliation[16] and chemical vapor deposition[17] developed for the controlled fabrication of thin layers of $TiSe_2$. The LTMDs have a variety of applications for studying the physics of competing phases as well as for their practical use as two-dimensional devices.

Here, we report the remarkable effects of chemical tuning on the transport properties of $TiSe_2$. A combination of Pt doping on the Ti sublattice, together with Se deficiency, in the series $Ti_{1-x}Pt_xSe_{2-y}$ results in the scaled resistivity changing by nearly 10 orders of magnitude. In particular, Se deficiency alone ($x = 0$, $y > 0$) completely suppresses the CDW transition and imparts a metallic character to the $y = 0.2$ system, resulting in a drop in the scaled low T resistivity by nearly two orders of magnitude. By contrast, Pt doping with no Se deficiency ($x > 0$, $y = 0$) hardly changes the CDW transition temperature, but reveals insulating behavior with (i) increasing high temperature ($T > T_{CDW}$) gap E_g and (ii) more then eight orders of magnitude increase of the resistivity scaled at 300 K for $x \leq 0.13$. A combination of Se deficiency and Pt doping ($y = 2x$, $x > 0$) shows a suppression of the CDW slower than in the former case ($y = 0$), but considerably faster then in the latter ($x = 0$), while the resulting high T resistivity ($T > T_{CDW}$) is metallic. The large range of resistivity values covered in $TiSe_2$ by a single (chemical) tuning parameter renders this system as a potential candidate for further exploring adequate transport properties for applications. Furthermore, the room temperature transport gap increasing with x makes this system ideal for transport gap engineering for devices. We argue that the transport properties are driven by the changing chemical potential with x and y, with band structure calculations qualitatively support this scenario. Theoretical calculations similar to these may aid in the future choice of chemical tuning parameters to control the targeted properties of $TiSe_2$.

II. METHODS

Polycrystalline samples of $Ti_{1-x}Pt_xSe_{2-y}$ were synthesized for various x and y using solid state reaction. Stoichiometric amounts of Pt, Ti and Se powders were sealed under vacuum in a silica tube. Reaction temperatures up to 1000°C were necessary to eliminate impurity phases such as Pt and $PtSe_2$, but this high temperature caused some Se evaporation. The mass difference before and after heating was compensated for by the addition of Se to the mixture, which was then heated at 650°C first in powder form, and then in pellet form, for several days,

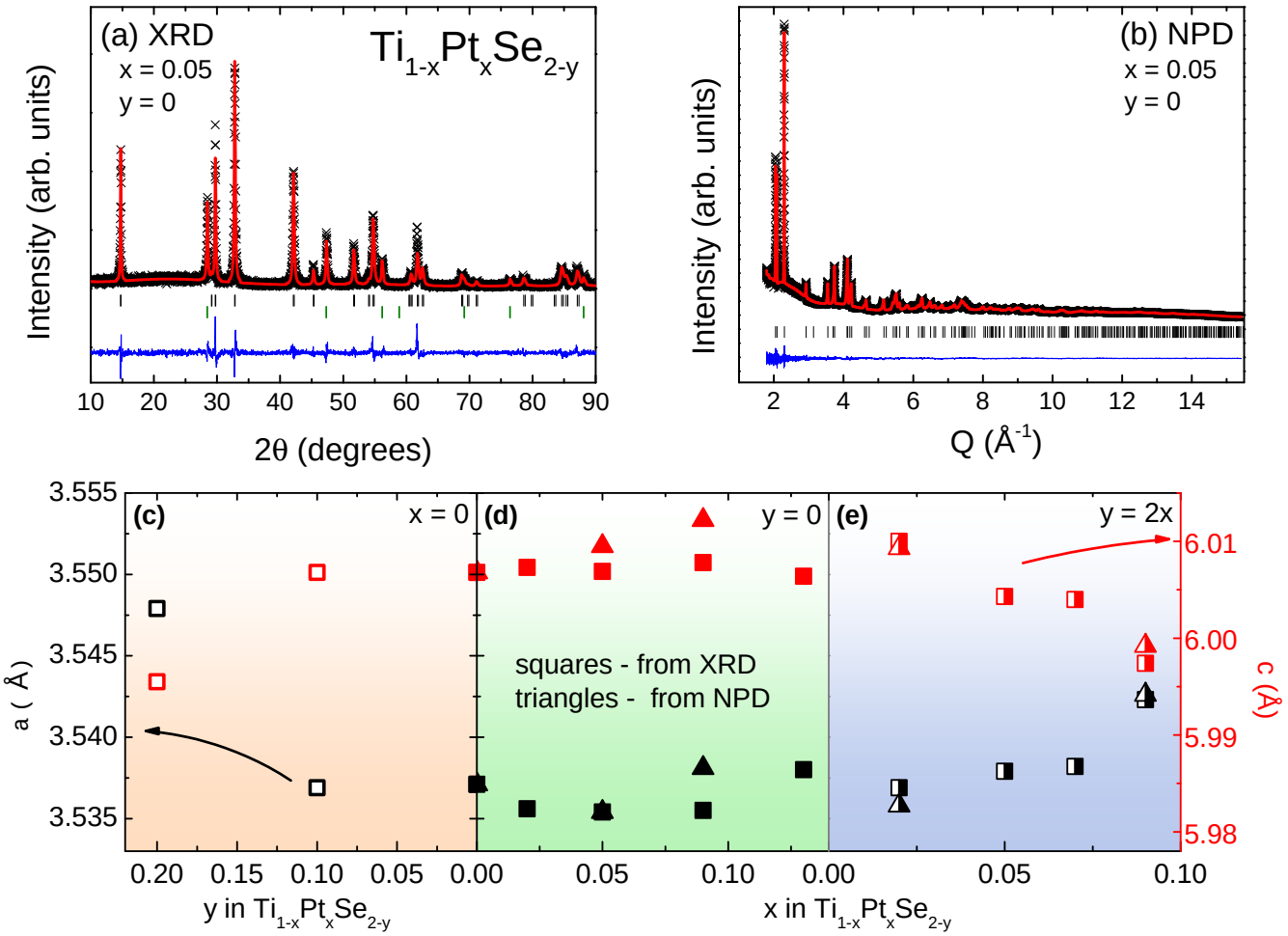

FIG. 1. (a) $Ti_{1-x}Pt_xSe_{2-y}$ XRD pattern for (x,y) = (0.05,0), with calculated peak positions marked by black (top) vertical liens. Green (bottom) vertical lines mark the Si standard peak positions. (b) Normalized $Ti_{1-x}Pt_xSe_{2-y}$ NPD pattern for (x,y) = (0.05,0). The refined lattice parameters from XRD (squares) and NPD (triangles) for $Ti_{1-x}Pt_xSe_{2-y}$ are shown for (c) x = 0 (no Pt), (d) y = 0 (no Se deficiency) and (e) y = 2x (Pt doping and Se deficiency). The refined lattice parameters from NPD were calibrated with those from XRD for (x,y) = (0,0).

with an intermediate grinding. The full procedure was carried out up to two times. A control $TiSe_2$ sample was synthesized following the same protocol, and the Ti:Se = 1:2 stoichiometry was confirmed by the resistivity peak height.[18] It appears that the $PtSe_2$-$TiSe_2$ solubility limit is reached in the region of $0.13 < x < 0.25$, since samples made with $x \geq 0.25$ show significant amounts of both binary phases.

Phase determination of the samples was done with powder x-ray diffraction (XRD) using a Rigaku D/max ULTIMA II diffractometer with a Cu $K\alpha$ radiation source. Rietveld analysis was performed using the GSAS/EXPGUI suite of programs.[19] For consistency, Si powder was used as standard in all XRD powder measurements. Neutron powder diffraction (NPD) was performed at room temperature, for (x,y) = (0,0), (0.02,0.04), (0.05,0), (0.09,0.18) and (0.09,0), using the time-of-flight HIPPO instrument at the Los Alamos Neutron Science Center (LANSCE). For the analysis, high resolution data was taken from the back scattering bank at a nominal diffraction angle of 144.447 deg. Electrical transport measurements were performed down to T = 2 K with a Quantum Design (QD) Physical Properties Measurement System (PPMS) using a standard four probe technique. Band structure calculations were performed with full potential linearized augmented plane wave (FP-LAPW) method implemented in the WIEN2K package.[20] A 10*10*10 k-point grid was used, together with the -6.0 Ryd separation energy between the core and valence states. A plain density functional theory (DFT) calculation with a localized exchange interaction did not reproduce the small 0.15 eV band gap in $TiSe_2$ that was observed in scanning tunneling spectroscopy (STS) data.[21] Therefore, a screened hybrid functional YS-PBE0[22] was used as the exchange-correlation potential, reproducing the band gap as with the GW calculation.[21] Pt-doped and Se-deficient samples calculations were performed by constructing supercells with a unit cell of ($2a$,$2a$,c) with one Ti atom replaced by Pt or one Se atom removed from the supercell.

III. DATA AND ANALYSIS

$TiSe_2$ has rather unique properties among the many known LTMDs. This compound displays a commensurate CDW, with long-debated properties of the normal state because of the small indirect gap in $TiSe_2$. It was difficult to unambiguously discern between a positive (semiconductor)[21,23,24] and a negative (semimetal)[25,26] gap, with the most recent scanning tunneling spectroscopy (STS) studies favoring a small band gap semiconductor.[21] The CDW transition around T_{CDW} = 220 K is marked by a broad peak in resistivity, without a preceding incommensurate CDW state as is the case in many LTMDs.[2,4,6,26] Unlike many other LTMDs, the CDW state in $TiSe_2$ does not result from Fermi surface nesting, but has been claimed to originate from an excitonic insulator state.[2,23,25] Most intriguing, $TiSe_2$ does not have a superconducting state above 0.4 K,[4] as is the case in many LTMDs, but a superconducting state can be induced either by the intercalation of transition metals T = Cu or Pd[4,6] or pressure.[27]

The transition metals M known to intercalate in $TiSe_2$ do not form stable MSe_2 compounds isostructural with $TiSe_2$. However the $PtSe_2$ and $TiSe_2$ are known isostructural LTMDs.[28] It is therefore not surprising that Pt is found to dope in place of Ti rather than intercalate in-between the layers.[28–31] Structural studies with XRD and NPD indeed confirm that this is the case in all $Ti_{1-x}Pt_xSe_{2-y}$ samples presented here. As an example, the refined XRD and NPD data for $Ti_{0.95}Pt_{0.05}Se_2$ are shown in Fig. 1. The XRD refinement confirms the $P\bar{3}m1$ space group for $Ti_{1-x}Pt_xSe_{2-y}$ for all reported (x,y) values. The lattice parameters a and c are plotted in Fig. 1c - e, both as a function of y (x = 0, open symbols, increase to the left, Fig. 1c), and as a function of x (for y = 0, full symbols, Fig. 1d, and for y = 2x, half-full symbols, Fig. 1e). Without doping (x = 0, open symbols), the lattice parameters $a(c)$ increases(decreases) for Se deficiency close to y = 0.2 (Fig. 1c). A similar effect occurs with doping *and* Se deficiency, when y = 2x (Fig. 1e). Surprisingly, it would appear that the amount of Pt is irrelevant from a structural perspective, given that the change in both a and c for y = 2x is the same as when the composition is only changed by Se deficiency y, for the same values of y (Fig 1c and e). This is also consistent with the fact that the lattice parameters remain virtually unchanged by doping alone (y = 0) for x values up to 0.13 (Fig. 1d).

To determine the location of the Pt atoms, several structure models were used for the NPD refinement. From GSAS refinements, a model with Pt and Ti sharing the same site appears to be the most accurate. Attempts to employ an intercalation model (with the Pt atoms located in the van der Waals gaps) consistently lead to values for Se occupancy and atomic displacements U_{iso} that were non-physical. Se occupancy increased to ~ 1.5, indicating 50% more Se occupying a site than physically possible. The U_{iso} for Pt in the van der Waals gap was 0.6 - 0.8, an order of magnitude larger than the typical U_{iso} values. This represented an implausible increase from room temperature U_{iso} values in crystals, usually on the order of 0.01, with higher values of 0.1 - 0.2 for loosely-bound atoms in organic molecules.[32] Therefore, it is concluded that Pt is not located in the van der Waals gap, but is only partially substituting on the Ti sites.

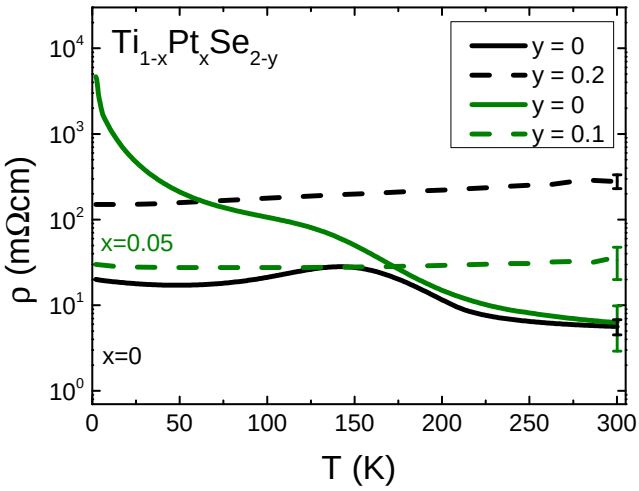

FIG. 2. The temperature dependent resistivity for $Ti_{1-x}Pt_xSe_{2-y}$ with x = 0 and x = 0.05 with no Se deficiency (y = 0, solid lines) and with Se deficiency (y > 0, dashed lines).

The effects of Se deficiency ($y \geq 0$) versus Pt doping ($x \geq 0$) on the transport properties are first illustrated by the change in the absolute resistivity values in Fig. 2. At T = 300 K, the resistivity ρ appears to increase one or two orders of magnitude from the y = 0 samples (solid lines) to the y > 0 samples (dashed lines). Furthermore, the qualitative temperature dependence of the resistivity is substantively different for the two sets of samples. The Se deficient samples (dashed lines) display a decreasing resistivity with decreasing temperature, indicative of a trend towards metallicity. Se deficiency has been shown to suppress the height of the peak below the CDW transition in $TiSe_{2-y}$ single crystals,[18] however without moving the CDW transition itself. The difference between the reported resistivity of Se-deficient single crystals and the polycrystalline samples in the current study is most likely in the actual amount of Se deficiency, which may differ from the nominal amounts y.

A comparison of the resistivity data, scaled at T = 300 K, for various x and y values for $Ti_{1-x}Pt_xSe_{2-y}$ is shown in Fig. 3. With no Pt doping, (x = 0, Fig. 3a), the resistivity displays metallic behavior when y = 0.2, with only small changes to resistivity for $y \leq 0.1$. As seen in the inset and below in Fig. 4a, as the resistivity displays metallic behavior, it appears that the CDW transition has been suppressed to below 2 K for this composition. In the case of Pt doping with no Se deficiency (y = 0, Fig 3b), the scaled resistivity increases by up to eight orders of magnitude, as x increase up to x = 0.13.

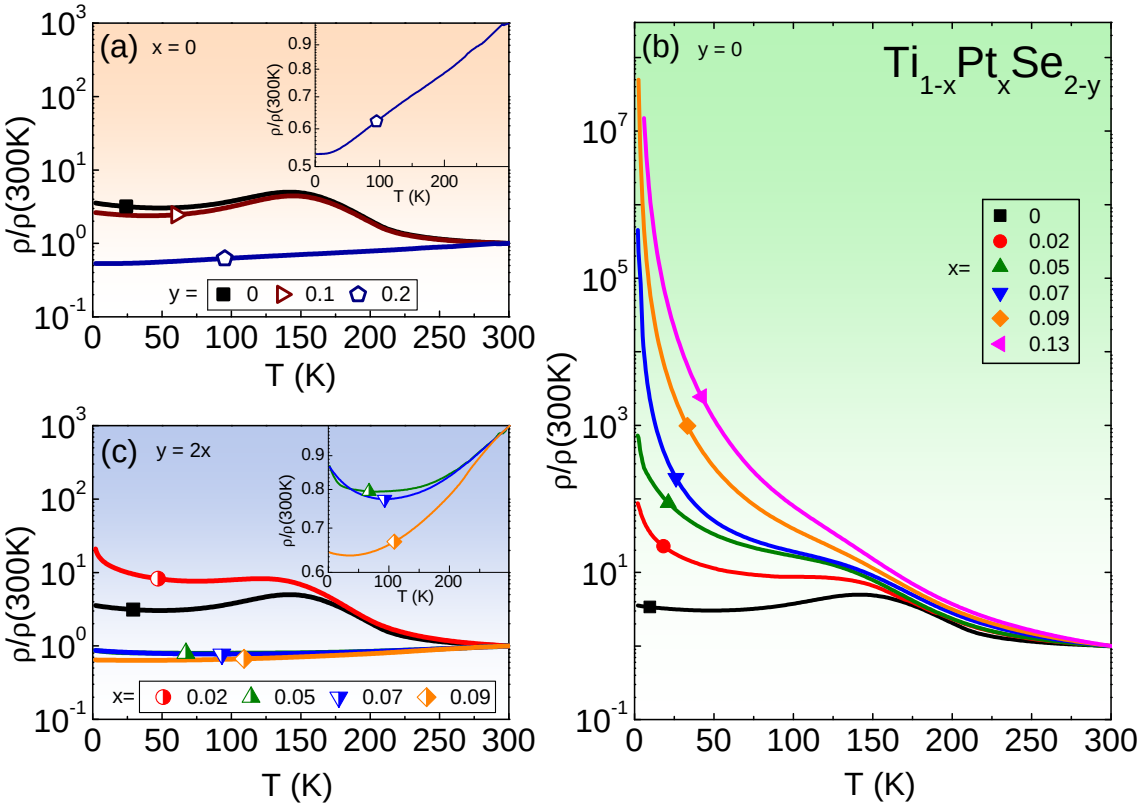

FIG. 3. Temperature-dependent resistivity scaled at 300 K $\rho/\rho(300K)$ for $Ti_{1-x}Pt_xSe_{2-y}$ for (a) x = 0 (no Pt), (b) y = 0 (no Se-deficiency) and (c) y = 2x (Pt and Se deficiency). The insets of (a) and (c) show details of the resistivity of the metallic phases.

Quantitatively, this can be described with an exponent α introduced as:

$$\rho(300K)/\rho(6K) = 10^{-\alpha} \quad (1)$$

The T = 6 K was used for defining α since, at lower temperatures, the resistance values for the most insulating sample (x = 0.13) surpassed the instrument limit for these measurements. The exponent α determined using Eq. 1 is maximum, $\alpha = 7.2$, for x = 0.13. However it is readily apparent from Fig. 3b that this is an underestimate for α, since ρ is likely to still increase rapidly below 6 K. Remarkably, the CDW transition appears minimally affected by Pt doping without Se deficiency, as will be shown below by the resistivity derivative plots (Fig. 4).

In the case of y = 2x (Fig. 3c), the low temperature scaled resistivity first shows a slight increase for x = 0.02 (circle), slower than that for the analogous x value with no Se deficiency (Fig. 3b). However, for x $\geq$ 0.05 the resistivity becomes metallic at high temperatures, while the CDW persists up to x = 0.05, albeit at decreasing temperatures. A competition appears to exist between Pt doping, which drives the system towards an insulating state, and the Se deficiency, which suppresses the CDW and induces a poor metal state. The CDW transition is more evident in the resistivity derivative $d\rho/dT$ (Fig. 4), with T_{CDW} defined as the temperature where a drop in the derivative occurs on cooling.[6] As mentioned above, the CDW is completely suppressed in the (x,y) = (0,0.2) sample (pentagon, Fig. 4a) or partially suppressed for (x,2x) with x $\geq$ 0.05 (Fig. 4c). All other compositions, and in particular those with no Se deficiency (Fig. 4b) display a CDW transition at the same temperature $T_{CDW} \approx 220$ K, marked by a vertical dashed line in Fig. 4. However, the CDW transition temperature is suppressed by nearly one order of magnitude for x = 0.05 in $Ti_{0.05}Pt_{0.95}Se_{1.9}$ (up-triangle, inset, Fig. 4c), down to $\sim$ 25 K.

For the insulating samples (y = 0, Fig. 3b), the band gap E_g above T_{CDW} was estimated using:[33]

$$\rho \propto e^{-\frac{E_g}{2k_BT}} \quad (2)$$

The gap E_g as a function of x (Fig. 5) is determined as the slope of the linear fits for $\ln\rho$ *vs.* $1/T$ (inset) above $T = 250$ K. The gap E_g increases linearly with x and reaches a maximum value $E_g = 125$ meV at x = 0.13.

In order to understand how tuning x and y produces the semiconducting and metallic states of $Ti_{1-x}Pt_xSe_{2-y}$, hybrid functional DFT calculations are performed for (x,y) = (0,0), (0.25,0) and (0,0.25). A density of states (DOS) plot is shown in Fig. 6. The calculations reveal $E_g = 0.2$ eV for $TiSe_2$, which agrees with the previous DFT calculations using the GW approximation,[34,35] and

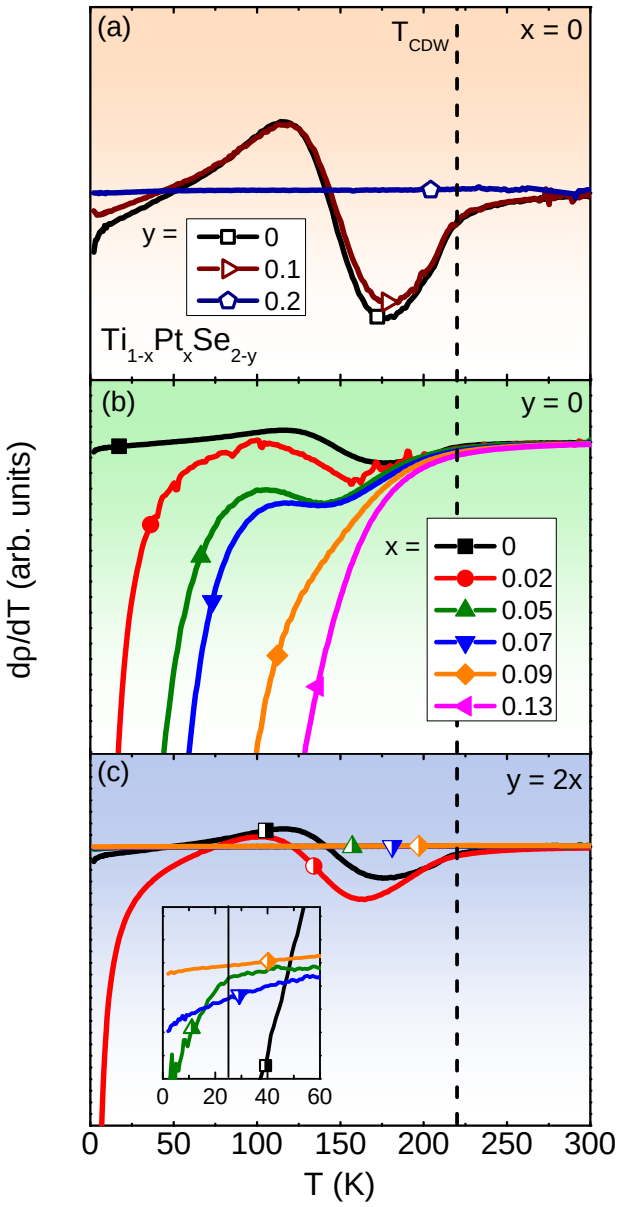

FIG. 4. Temperature derivatives of the resistivity $d\rho/dT$ for $Ti_{1-x}Pt_xSe_{2-y}$ for (a) x = 0 (no Pt), (b) y = 0 (no Se deficiency), (c) y = 2x (Pt and Se deficiency). The inset in (c) is the low temperature region for y = 2x.

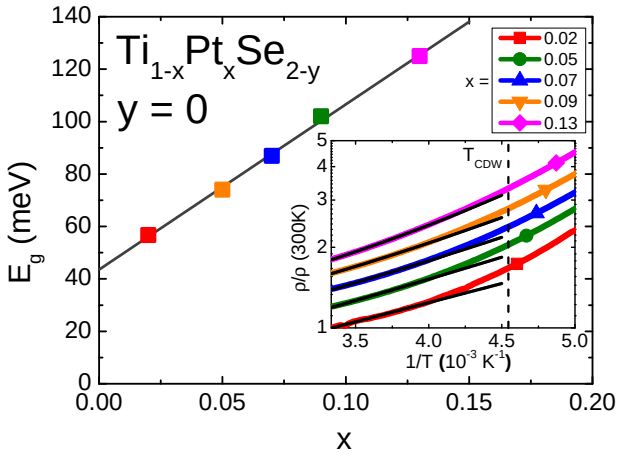

FIG. 5. Band gap E_g as a function of Pt concentration x in $Ti_{1-x}Pt_xSe_{2-y}$. Inset: linear fits of $\ln\rho$ vs $1/T$ above 250 K were used to determine E_g.

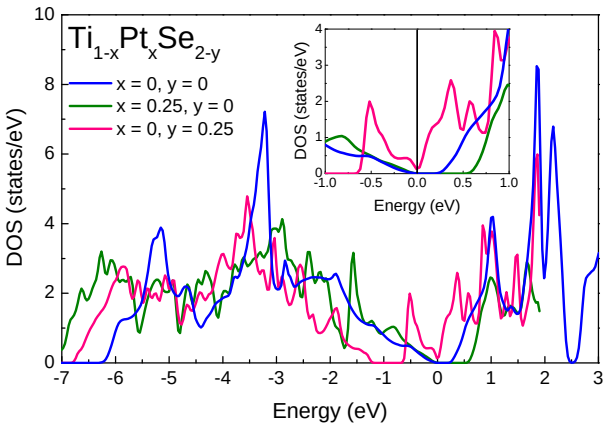

FIG. 6. Hybrid functional DFT calculations for (x,y) = (0,0),(0.25,0) and (0,0.25). Inset: the details near the Fermi energy reveal small but finite DOS only for the (x,y) = (0,0.25) sample.

close to some of the recent experimental estimates.[2,25,36] Pt doping alone (x,y) = (0.25,0) increases the gap to E_g = 0.5 eV, a trend consistent with the observed linear change in E_g.

The valence band is between -6 eV and 0 eV for (x,y) = (0,0), and widens with Pt doping by about 1 eV in (x,y) = (0.25,0). This widening is possibly due to the smaller electronegativity difference between Pt and Se (0.35) compared to Ti and Se (1.01).[37] However, Se deficiency in (x,y) = (0,0.25) does not broaden the valence band, but instead shifts it down by 1 eV. The Ti 3d electron band shifts to the Fermi level, resulting in a finite DOS in (x,y) = (0,0.25), albeit with a small value (local minimum) at E_F. The Se deficiency can be understood as analogous to electron doping, as fewer Ti electrons are transferred to Se sites in (x,y) = (0,0.25) compared to (x,y) = (0,0).

The Ioffe-Regel limit specifies the maximum resistivity of a metal. The limit is estimated from the Drude transport equation $\rho = ne^2\tau/m$, using the Fermi velocity (assuming a spherical Fermi surface) for estimating the mean scattering time τ, with the Fermi surface taking up the entirety of the first Brillouin zone to estimate the charge density n, and using the electron's rest properties for the values of e and m. The large increase in resistivity for the Se-deficient samples, which violates the Ioffe-Regel limit of 500 $\mu\Omega$cm (calculated for a nearly full first Brillouin zone with a typical lattice spacing of $\approx$ 4 Å),[38] cannot be explained by the small DOS alone. The large resistivity could be indicative of

other sources of electron scattering such as from underlying CDW correlations,[39,40] or the electrons becoming strongly localized, as is the case in some bad metals.[41]

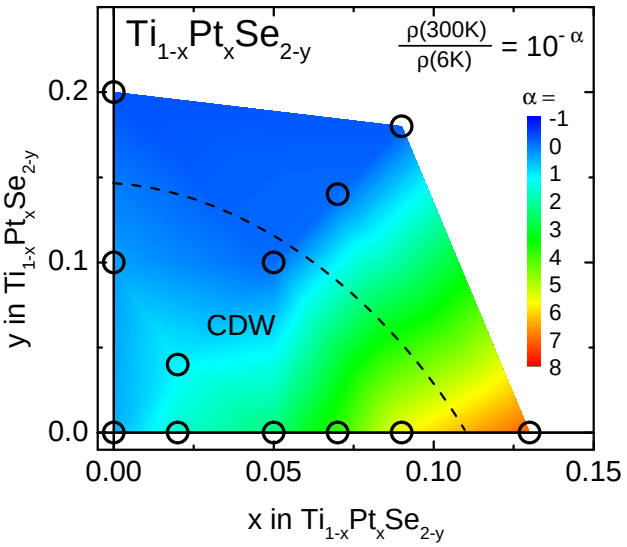

FIG. 7. x - y contour plot of the resistivity exponent α (see text). Symbols: actual data determined from $\rho(T)$ data; dashed line: possible boundary for the CDW state.

The overall effects of Pt doping and Se deficiency are summarized in the (x,y) contour plot of the resistivity exponent α (eq. 1) in Fig. 7. It is readily apparent that the two chemical control parameters x and y have drastically different effects on the transport properties of $TiSe_2$. First, for y = 0, α increases linearly with x up to $\alpha \approx 8$ for x = 0.13. The opposite trends, albeit much slower, is revealed by Se deficiency without Pt doping (x = 0), where α decreases with y to $\alpha \approx -1$ for y = 0.2. Along the line y = 2x, the competition between the two chemical control parameters x and y results in a non-monotonous change in α. For low x, Pt doping wins over Se deficiency as the x = 0.02 sample becomes slightly more semiconducting than the x = 0 one. Further increasing x in the case of y = 2x results in decreasing α and a metallic state towards high x. The y = 2x delineates a metallic range above, with increasing insulating character upon approaching the x axis at high x. Interestingly, the CDW state seems to be less sensitive to the change in the electrical resistivity. The dashes line in Fig. 7 indicates that the CDW state persists for most semiconducting samples. The nearly divergent ρ for (x,y) = (0.13,0) makes it very difficult to still determined the signature of the CDW, while in the (x,2x) samples with x $\leq$ 0.07, downturns in $d\rho/dT$ close to the lowest measured T (inset, Fig. 4c) suggest that a CDW transition might still occur just below 2 K. This would be consistent with the trend observed up to x = 0.05, where T_{CDW} has been suppressed down to 25 K.

IV. DISCUSSION AND CONCLUSIONS

In $Ti_{1-x}Pt_xSe_{2-y}$, the x and y chemical control parameters drive changes from metallic to semiconducting behavior, simultaneous with changes of the a and c lattice parameters. Interestingly, the a increases and c decreases with increasing y in the undoped samples (x = 0 in Fig. 1c). The accompanying trend towards metallicity (Fig. 3a) might be associated with increasing inter-layer correlations, as the corresponding lattice parameter c becomes smaller. By contrast, changing x with no Se deficiency (y = 0 in Fig. 1d) leaves a and c virtually unchanged, while the transport properties are dramatically affected (Fig. 3b). In conjunction with the band structure calculations, these observations indicate that Se deficiency shifts the chemical potential of the system towards the Ti 3d bands and increases, at least crystallographically, the 3D character of these compounds as a increases and c decreases. Previously, Cu and Pd intercalation in $TiSe_2$ also led to an increase of the a lattice parameter, resulting in metallic (and eventually superconducting) behavior.[4,6] However, the c lattice parameters for the intercalated superconducting compounds increased, contrary to the effect in the current Pt-doped samples. A more thorough exploration of the (x,y) phase space is necessary to fully determine the correlations between the electronic and structural properties of $TiSe_2$. It is of note, however, that even $TiSe_2$ intercalation with transition metals that did not yield a low temperature superconducting state[42] resulted in an expected decrease of the inter-layer spacing c.

Previous experimental studies on $PtSe_2$ indicated that this dichalcogenide compound was a semiconductor with $E_g = 100$ meV,[31] while $TiSe_2$ was likely a semiconductor with a small (≈ 20 meV) band gap E_g.[2,21,23–25] Considering that the Ti and Pt are chemically and electronically substantively different, it is not entirely unexpected that the change in the gap value with x is non-monotonic. Pt doping of only 13% in $TiSe_2$ (Fig. 3b) appears to increase the gap beyond that of pure $PtSe_2$, suggesting a higher maximum gap in $Ti_{1-x}Pt_xSe_{2-y}$, if higher compositions were not precluded by the solubility of the two end compounds. Interestingly, the CDW is observed to persist in the semiconducting state in $Ti_{1-x}Pt_xSe_{2-y}$ (y = 0), as seen in Fig. 3b. This was also the case in Pd-intercalated $TiSe_2$.[6] However, in the latter case, much smaller scaled resistivity values ($\rho/\rho(300K) \leq 10^3$) favored a superconducting state for high enough Pd composition. However, given that the gap in $TiSe_2$ is very small, there is an ongoing debate over its exact value,[2,18,21,23–26,36] which is irrelevant for the current discussion.

Engineering a transport gap in $TiSe_2$ may allow transistors and other electronic devices to be made based on $TiSe_2$.[12,13,43] While the band gap in the bulk is smaller than the ideal 1 eV for some applications (*e.g.* photovoltaic cells[44]), the band gap of dichalcogenides has been raised by 0.5 eV for MoS_2 once the samples were exfoliated to a single monolayer.[43] Additionally, for any prac-

tical device using the CDW state, the CDW would have to exist at room temperature.[16] Previous work showed that T_{CDW} could also be raised in thin layer samples of $TiSe_2$.[16] Therefore a comparison of the properties of bulk and exfoliated $Ti_{1-x}Pt_xSe_{2-y}$ may lead to such a desirable band gap E_g and T_{CDW} increase. Such experiments are currently underway. Furthermore, tuning of the chemical parameters x and y makes $Ti_{1-x}Pt_xSe_{2-y}$ ideal for studies of the fundamental physics of the CDW state affected by both the band gap and dimensionality.

ACKNOWLEDGMENTS

The neutron scattering work at Rice was supported by the US DOE, BES, Contract No. DE-SC0012311 (P.D.). Part of the work is supported by the Robert A. Welch Foundation Grant No. C-1839 (P.D.) E.M. and J.S.C. acknowledge support from the DOD PECASE. This work has benefited from Lujan Neutron Scattering Center at LANSCE, which is funded by the U.S. Department of Energys Office of Basic Energy Sciences. Los Alamos National Laboratory is operated by Los Alamos National Security LLC under DOE contract DEAC52-06NA25396.

[1] J. A. Wilson and A. D. Yoffe, Advances in Physics **18**, 193 (1969).
[2] K. Rossnagel, Journal of Physics - Condensed Matter **23**, 213001 (2011).
[3] R. Ang, Y. Miyata, E. Ieki, K. Nakayama, T. Sato, Y. Liu, W. J. Lu, Y. P. Sun, and T. Takahashi, Physical Review B **88**, 115145 (2013).
[4] E. Morosan, H. W. Zandbergen, B. S. Dennis, J. W. G. Bos, Y. Onose, T. Klimczuik, A. P. Ramirez, N. P. Ong, and R. J. Cava, Nature Physics **2**, 544 (2006).
[5] K. E. Wagner, E. Morosan, Y. S. Hor, J. Tao, Y. Zhu, T. Sanders, T. M. McQueen, H. W. Zandbergen, A. J. Wiliams, D. V. West, and R. J. Cava, Physical Review B **78**, 104520 (2008).
[6] E. Morosan, K. E. Wagner, L. L. Zhao, Y. Hor, A. J. Wiliams, J. Tao, Y. Zhu, and R. J. Cava, Physical Reveiw B **81**, 094524 (2010).
[7] J. J. Yang, Y. J. Choi, Y. S. Oh, A. Hogan, Y. Horibe, K. Kim, B. I. Min, and S. W. Cheong, Physical Review Letters **108**, 116402 (2012).
[8] E. Morosan, H. W. Zandbergen, L. Li, M. Lee, J. G. Checkelsky, M. Heinrich, T. Siegrist, N. P. Ong, and R. J. Cava, Physical Review B **75**, 104401 (2007).
[9] V. G. Pleschov, N. V. Baranov, A. N. Titov, K. Inoue, M. I. Bartashevich, and T. Goto, Journal of Alloys and Compounds **320**, 13 (2001).
[10] M. Koyano, M. Suezawa, H. Watanabe, and M. Inoue, Journal of the Physical Society of Japan **63**, 1114 (1994).
[11] B. Sipos, A. F. Kusmartseva, A. Akrap, H. Berger, L. Forro, and E. Tutis, Nature Materials **7**, 960 (2008).
[12] H. J. Conley, B. Wang, J. I. Ziegler, R. F. Haglund, S. T. Pantelides, and K. I. Bolotin, Nano Letters **13**, 3626 (2013).
[13] H. Qiu, L. J. Pan, Z. N. Yao, J. J. Li, Y. Shi, and X. Wang, Applied Physics Letters **100**, 123104 (2012).
[14] J. Khan, C. Nolen, D. Teweldebrhan, D. Wickramaratne, R. Lake, and A. Balandin, Applied Physics Letters **100**, 043109 (2012).
[15] J. Renteria, R. Samnakay, C. Jiang, T. R. Pope, P. Goli, Z. Yan, D. Wickramaratne, T. T. Salguero, A. G. Khitun, R. K. Lake, and A. A. Balandin, Journal of Applied Physics **115**, 034305 (2014).
[16] P. Goli, J. Khan, D. Wickramaratne, R. K. Lake, and A. A. Balandin, Nano Letters **12**, 5941 (2012).
[17] S. L. Benjamin, C. K. de Groot, C. Gurnani, A. L. Hector, R. Huang, K. Ignatyev, W. Levason, S. J. Pearce, F. Thomas, and G. Reid, Chemistry of Materials **25**, 4719 (2013).
[18] F. J. DiSalvo, D. E. Moncton, and J. V. Waszczak, Physical Review B **14**, 4321 (1976).
[19] A. C. Larson and R. B. Von Dreele, *General Structure Analysis System (GSAS)*, edited by L. A. N. Laboratory (2000) pp. LAUR 86–748.
[20] P. K. Blaha, K. Schwarz, G. Madsen, D. Kvasnicka, and J. Luitz, "Wien2k package," `http://www.wien2k.at`.
[21] M. Cazzaniga, H. Cercellier, M. Holzmann, C. Monney, P. Aebi, G. Onida, and V. Olevano, Physical Review B **85**, 195111 (2012).
[22] F. Tran and P. Blaha, Physical Review B **83**, 235118 (2011).
[23] M. M. May, C. Brabetz, C. Janowitz, and R. Manzke, Physical Review Letters **107**, 176405 (2011).
[24] T. E. Kidd, T. Miller, M. Y. Chou, and T. C. Chiang, Physical Review Letters **88**, 226402 (2002).
[25] H. Cercellier, C. Monney, F. Clerc, C. Battaglia, L. Despont, M. G. Garnier, H. Beck, P. Aebi, L. Patthey, H. Berger, and L. Forro, Physical Review Letters **99**, 146403 (2007).
[26] G. Li, W. Z. Hu, D. Qian, D. Hsieh, M. Z. Hasan, E. Morosan, R. J. Cava, and N. L. Wang, Physical Review Letters **99**, 027404 (2007).
[27] A. Kusmartseva, B. Sipos, H. Berger, L. Forro, and E. Tutis, Physical Review Letters **103**, 236401 (2009).
[28] R. M. A. Lieth and J. C. J. M. Terhell, "Preparation and crystal growth of materials with layered structures," (D. Reidel Publishing Company, 1977).
[29] F. Gronvold, H. Haraldsen, and A. Kjekshus, Acta Chemica Scandinavica **14**, 1879 (1960).
[30] S. Furuseth, K. Selte, and A. Kjekshus, Acta Chemica Scandinavica **19**, 257 (1965).
[31] F. Hulliger, Journal of Physics and Chemistry of Solids **26**, 639 (1965).
[32] W. Massa, *Crystal Structure Determination*, second edition ed. (Springer, 2004).
[33] N. W. Ashcroft and N. D. Mermin, *Solid State Physics* (Brooks/Cole, 1976).
[34] L. Hedin, Physical Review **139**, A796 (1965).
[35] G. Strinati, H. J. Mattausch, and W. Hanke, Physical Review B **25**, 2867 (1982).
[36] J. C. E. Rasch, T. Stemmler, B. Muller, L. Dudy, and R. Manzke, Physical Review Letters **101**, 237602 (2008).
[37] D. R. Lide, ed., *CRC Handbook of Chemistry and Physics*,

84th ed. (CRC Press, Boca Raton, Florida, 2003) section 9, Molecular Structure and Spectroscopy: Electronegativity.
[38] M. Gurvitch, Physical Review B **24**, 7404 (1981).
[39] M. Naito and S. Tanaka, Journal of the Physical Society of Japan **51**, 219 (1982).
[40] R. M. Fernandes, E. Abrahams, and J. Schmalian, Physical Review Letters **107**, 217002 (2011).
[41] J. Merino and R. H. McKenzie, Physical Review B **61**, 7996 (2000).
[42] E. Morosan, (Unpublished).
[43] Y. Yoon, K. Ganapathi, and S. Salahuddin, Nano Letters **11**, 3768 (2011).
[44] M. Moustafa, T. Zandt, C. Janowitz, and R. Manzke, Physical Review B **80**, 035206 (2009).